

# IP-UNet: Intensity Projection UNet Architecture for 3D Medical Volume Segmentation

Nyothiri Aung, Tahar Kechadi, Liming Chen and Sahraoui Dhelim

**Abstract**—CNNs have been widely applied for medical image analysis. However, limited memory capacity is one of the most common drawbacks of processing high-resolution 3D volumetric data. 3D volumes are usually cropped or downsized first before processing, which can result in a loss of resolution, increase class imbalance, and affect the performance of the segmentation algorithms. In this paper, we propose an end-to-end deep learning approach called IP-UNet. IP-UNet is a UNet-based model that performs multi-class segmentation on Intensity Projection (IP) of 3D volumetric data instead of the memory-consuming 3D volumes. IP-UNet uses limited memory capability for training without losing the original 3D image resolution. We compare the performance of three models in terms of segmentation accuracy and computational cost: 1) Slice-by-slice 2D segmentation of the CT scan images using a conventional 2D UNet model. 2) IP-UNet that operates on data obtained by merging the extracted Maximum Intensity Projection (MIP), Closest Vessel Projection (CVP), and Average Intensity Projection (AvgIP) representations of the source 3D volumes, then applying the UNet model on the output IP images. 3) 3D-UNet model directly reads the 3D volumes constructed from a series of CT scan images and outputs the 3D volume of the predicted segmentation. We test the performance of these methods on 3D volumetric images for automatic breast calcification detection. Experimental results show that IP-UNet can achieve similar segmentation accuracy with 3D-UNet but with much better performance. It reduces the training time by 70% and memory consumption by 92%.

**Index Terms**—Maximum Intensity Projection, MIP, Medical image segmentation, 3D volumes, Memory optimization, Memory bottleneck.

## I. INTRODUCTION

Deep convolution neural networks (CNN) have proven their efficiency for image analysis, such as Deep convolution neural networks (CNN) have proven their efficiency for image analysis, such as image classification and image segmentation [1]. CNNs have been widely applied successfully for medical image analysis. Particularly UNet [2], a CNN architecture, had achieved satisfactory results in medical image segmentation. Medical images such as Computed Tomography (CT) and Magnetic Resonance Imaging (MRI) are represented as 3D volumes rather than 2D images. Therefore, there are 3D variants of CNN architectures, such as 3D-CNN [3] and 3D-UNet [4]. These 3D models usually yield better accuracy, as they can capture the 3D-contextual information of volumetric data rather than individually processing CT/MRI slices. However, limited memory capacity is one of the most common drawbacks of processing high-resolution 3D volumetric data.

3D volumes are usually cropped or downsized first before processing. These operations can result in a loss of resolution and increase the class imbalance in the input data batches, which can affect the performances of segmentation algorithms. This problem is known as memory bottleneck [5].

Intensity projection in medical imaging is used to transform 3D images into 2D images for visualization purposes. For instance, we use maximum intensity projection (MIP) to project the voxel with the highest Hounsfield unit on a given axis throughout the volume onto a 2D image. MIP is effective for automatic pulmonary nodule detection [6], tumor detection [7], and rheumatoid arthritis detection [8], to name a few. Local maximum intensity projection (LMIP), also known as Closest Vessel Projection (CVP), was proposed to improve MIP. LMIP selects the local maximum Hounsfield unit above a certain threshold rather than the absolute maximum, as in MIP. Average intensity projection (AvgMIP) [9] and Minimum intensity projection (MinIP) [10] are also widely used in medical imaging. In this paper, we leverage intensity projection to perform segmentation on the projection of 3D volumes without loss of precision introduced by cropping or downsizing. Our contributions can be summarized as follows:

- We propose IP-UNet, an end-to-end deep learning model that operates on intensity projections of 3D volumes instead of the memory-consuming 3D volumetric data. IP-UNet can be trained with limited memory capability without loss of resolution of the original 3D images.
- We compare the performance of IP-UNet in terms of segmentation accuracy and computational cost with similar baselines, namely, UNet and 3D-UNet.
- We train and evaluate IP-UNet on 500 3D volumetric images for automatic breast calcification detection.

The rest of the paper is organized as follows: Section II reviews the related literature. In Section III, we present the proposed IP-UNet architecture. In Section IV, we compare IP-UNet to similar models regarding segmentation accuracy and computational cost. Finally, Section V concludes the paper.

## II. RELATED WORK

Many previous works have studied computational and memory efficiency when dealing with 3D volumetric data.

Kozinski et al. [11], [12] introduced a loss function for deep neural networks that can be used for 3D volumetric data segmentation. They proposed annotating 2D projections of the training 3D volumes, which reduces the amount of effort needed to annotate the volumes. Their results show that only

Nyothiri Aung, Tahar Kechadi and Sahraoui Dhelim are with the School of Computer Science, University College Dublin, Ireland.

Liming Chen is with the School of Computing, Ulster University, U.K.

a marginal accuracy loss is introduced by their method, by in return they get a considerable reduction in annotation effort. Wang et al. [13] proposed a two-stage Unet framework that simultaneously learns to identify a Region of Interest (ROI) within the entire 3D volume and to classify voxels without losing the original resolution. Their proposed method classifies all the voxels viewed from an axial slice based on a pre-defined neighborhood of axial slices around it.

Similarly, Zheng et al [14], [15] trained separately various deep-learning models using the MIP of CT images with different slab thicknesses. They concluded that for a single slab thickness, MIP images of 10 mm are the most effective for lung nodule detection. Specifically, The sensitivity increased (82.8% to 90.0%) for slab thickness of 1 to 10 mm and decreased (88.7% to 76.6%) for slab thickness of 15–50 mm. Their results proved that the use of images with multiple MIP settings can improve the performance at the nodule candidate detection stage. Furthermore, the optimal MIP slab thickness in their deep-learning model was similar to the one commonly used by radiologists in the clinic. Fujioka et al. [16], [17] compared the performance of various CNN models (DenseNet121, DenseNet169, InceptionResNetV2, InceptionV3, NasNetMobile, and Xception) when applied to MIP of dynamic contrast-enhanced breast MRI images. They find out that operating CNN on MIP can achieve up to 98% AUC. Wang et al [18] applied ResNet-50 with the axial and sagittal MIP of early post-contrast subtracted breast MRI images. Their system achieved comparable diagnostic performance with the senior radiologist and outperformed the junior radiologist. Song et al [19] proposed a 3d-UNet segmentation network for coronary artery detection, which is able to extract and fuse rectifying features efficiently. They used dense blocks in 3D-UNet for the encoding process to obtain rich representative features related to coronary artery segmentation; and 3D residual blocks with feature rectification capability are used to improve the segmentation accuracy. Similarly, Lei et al [20] introduced a 3D attention fully convolution network (FCN) method for automatic segmentation of the coronary artery. FCN was employed to operate end-to-end mapping from coronary computed tomographic angiography images to the binary segmentation of coronary artery. Deep attention strategy was used to highlight the informative semantic features extracted from CCTA image and to improve the segmentation accuracy.

### III. IP-UNET ARCHITECTURE

The general architecture of IP-UNet is shown in Figure 1. IP-UNet takes the 3D volumetric image as input, and applies three intensity projection functions on the sagittal axis of the 3D volume, namely LMIP, AvgIP and MIP, as shown in eq(1), eq(2) and eq(3) respectively. Where,  $v_{i,j}$  is the projected voxel in the new 2D image in position  $(i, j)$ , and  $v_{i,j,k}$  is the voxel the 3D image in position  $(i, j, k)$ , and  $x$  is the local maximum intensity threshold for CVP. It is worth noting that we applied intensity projection functions of the sagittal axis because coronary artery calcification is salient from the sagittal view. Intensity projection functions can be

also applied on the coronal axis or axial axis depending on the use case. For instance, in the context of brain image analysis, applying intensity projection function on the axial axis could be most applicable. Figure 2 shows the neural network architecture IP-UNet. The encoder and decoder phases follow the original U-Net model. Each encoding level includes two  $3 \times 3$  convolutions operators, each operator is followed by a batch normalization and a Leaky ReLU operation. We leverage LeakyReLU [21], instead of ReLU function used in the original UNet, to mitigate the dying Relu problem, where most of the neural neurons are set to zero because of negative inputs during the learning process. For down-sampling, each encoding level is followed by a  $2 \times 2$  max pooling operation with the stride of two, Followed by convolution operations that double the feature channel count as detailed in Table I. In each decoding level, the height and width of the feature maps is doubled through up-sampling. Then the resulting block is concatenated with the corresponding feature maps block from the encoding phase.

$$CVP(v_{i,j}) = \begin{cases} \max([v_{i,j,0}, \dots, v_{i,j,k-1}]), & \text{if } \max \leq x \\ 0, & \text{Otherwise} \end{cases} \quad (1)$$

$$AvgIP(v_{i,j}) = \frac{\sum [v_{i,j,0}, \dots, v_{i,j,k-1}]}{\|[v_{i,j,0}, \dots, v_{i,j,k-1}]\|} \quad (2)$$

$$MIP(v_{i,j}) = \max([v_{i,j,0}, \dots, v_{i,j,k-1}]) \quad (3)$$

IP-UNet applies 2D UNet architecture on each of the composited 2D intensity projections. In our case, the input images are  $512 \times 512$ . Each of the 2D projections passes through encoding and decoding phases. In the encoding phase, each level includes  $3 \times 3$  convolutions, followed by batch normalization and ReLU. For each downsampling step,  $2 \times 2$  max pooling with a stride of 2 is applied. As shown in Table I, there are 14 layers in the encoding phase, 10 convolutional layers, plus 4 max pooling layers. In the decoding phase, the size of feature maps is doubled step through de-convolution and concatenation with copies from the decoding phase, which allows the fusing of shallow high-resolution features with deep semantic features. Table I shows the layers of encoding and decoding phases.

#### A. Loss function

Dice Loss has been proven as a suitable loss function for medical image segmentation. Dice Loss function is defined in eq(4):

$$DL(P, P') = 1 - \frac{2|P \cap P'|}{|P| + |P'|} \quad (4)$$

where  $P$  represents the predicted result, and  $P'$  represents the ground truth annotation. However, in our case, the proportion of calcified voxels among overall annotation voxels is very low, this could introduce class unbalance in the training process. Class unbalance can cause biased predictions, which may result in high specificity but low sensitivity. Prediction bias is unacceptable, especially in medical applications where false positives are much more tolerable compared to false

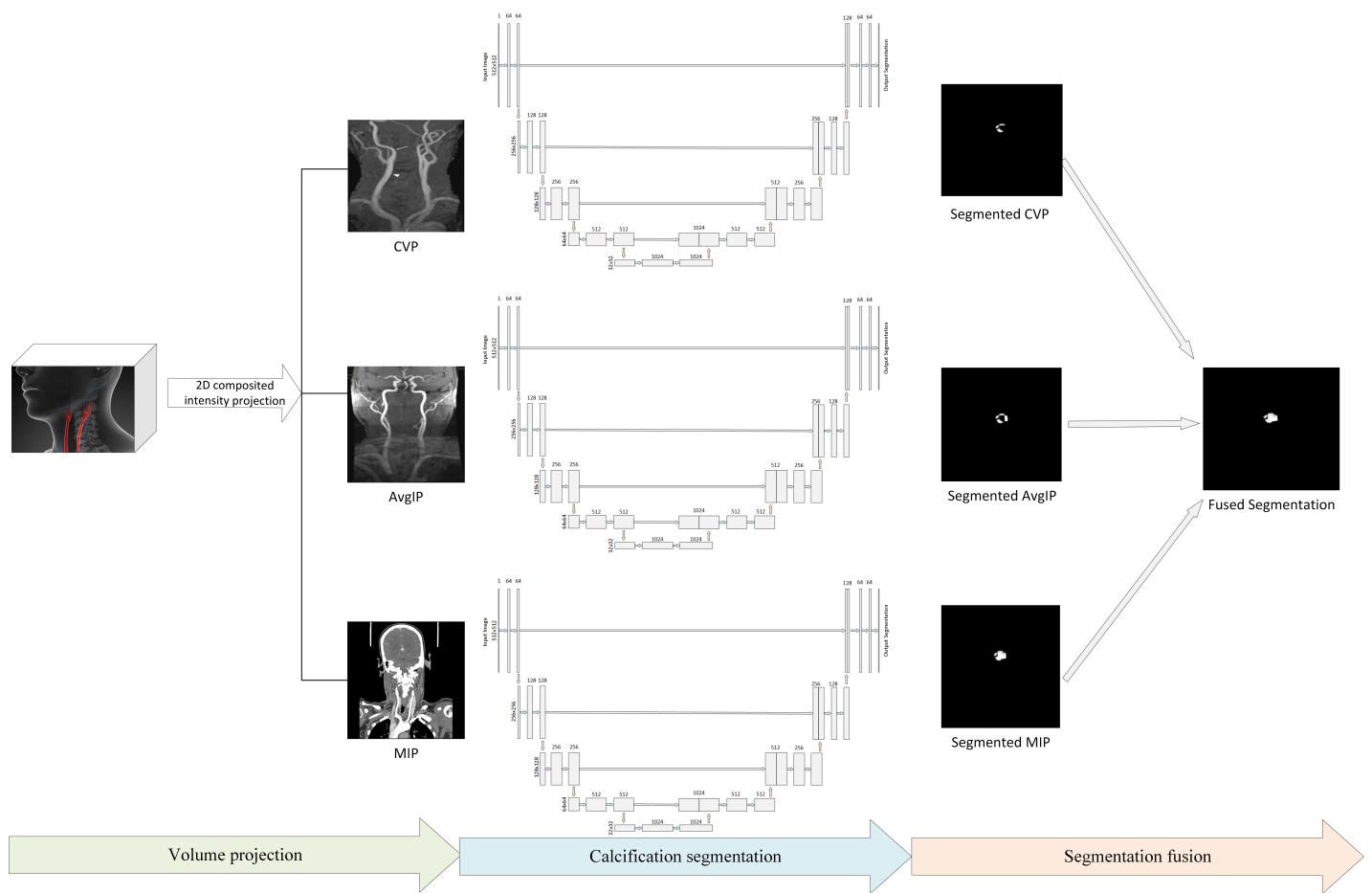


Fig. 1: IP-UNet overall architecture

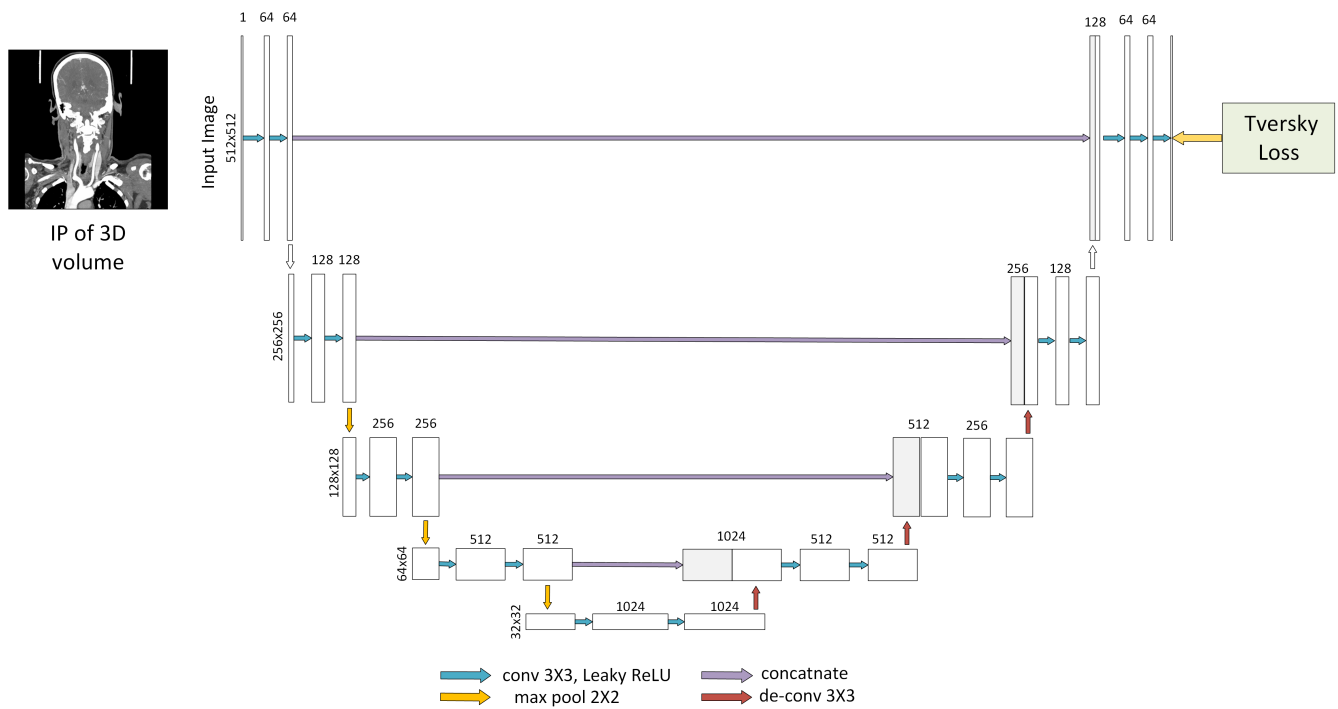


Fig. 2: IP-UNet layers architecture

TABLE I: IP-UNet network layers

No	Phase	Type	Input	Filter	Stride/Size	Output
1	Encode	conv	512X512X2	64	1/3X3	512X512X64
2	Encode	conv	512X512X64	64	1/3X3	512X512X64
3	Encode	max	512X512X64		2/2X2	256X256X64
4	Encode	conv	256X256X64	128	1/3X3	256X256X128
5	Encode	conv	256X256X128	128	1/3X3	256X256X128
6	Encode	max	256X256X128		2/2X2	128X128X128
7	Encode	conv	128X128X128	256	1/3X3	128X128X256
8	Encode	conv	128X128X256	256	1/3X3	128X128X256
9	Encode	max	64X64X256		2/2X2	64X64X256
10	Encode	conv	64X64X512	512	1/3X3	64X64X512
11	Encode	conv	64X64X512	512	1/3X3	64X64X512
12	Encode	max	32X32X512		2/2X2	32X32X512
13	Encode	conv	32X32X1024	1024	1/3X3	32X32X1024
14	Encode	conv	32X32X1024	1024	1/3X3	32X32X1024
15	Decode	deconv	32X32X1024	512	2/3X3	64X64X512
16	Decode	concat	64X64X512			64X64X1024
17	Decode	conv	64X64X1024	512	1/3X3	64X64X512
18	Decode	conv	64X64X512	512	1/3X3	64X64X512
19	Decode	deconv	64X64X512	256	2/3X3	128X128X256
20	Decode	concat	128X128X512			128X128X512
21	Decode	conv	128X128X512	256	1/3X3	128X128X256
22	Decode	conv	128X128X256	256	1/3X3	128X128X256
23	Decode	deconv	128X128X256	128	2/3X3	256X256X128
24	Decode	concat	256X256X128			256X256X256
25	Decode	conv	256X256X256	128	1/3X3	256X256X128
26	Decode	conv	256X256X128	128	1/3X3	256X256X128
27	Decode	deconv	256X256X128	64	2/3X3	512X512X64
28	Decode	concat	512X512X64			512X512X128
29	Decode	conv	512X512X128	64	1/3X3	512X512X64
30	Decode	conv	512X512X64	64	1/3X3	512X512X64
31	Decode	conv	512X512X64	3	1/1X1	512X512X3

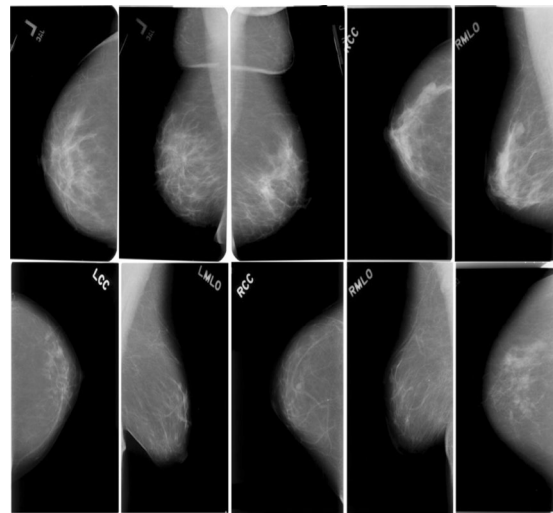


Fig. 3: Example of scans from CBIS-DDSM dataset

TABLE II: Dataset statistics

Parameter	Value
Number of patients	753
Benign cases (Training)	329
Malignant Cases (Training)	273
Benign cases (Testing)	85
Malignant Cases (Testing)	66

negatives. Several methods have been proposed to deal with this problem including balanced sampling, two-step training, sample re-weighting, and similarity loss functions. To address the class imbalance effect [22], we have also Tversky loss function [23] as defined in eq(5)

$$TL(P, P') = 1 - \frac{|P \cap P'|}{|P \cap P'| + \alpha|P - P'| + \beta|P' - P|} \quad (5)$$

where  $\alpha$  and  $\beta$  are the hyperparameters that are used to tune false negative and false positive toleration rates, which must satisfy  $\alpha + \beta = 1$ . When  $\alpha = \beta = 0.5$ , Tversky loss is the same as the Dice loss

#### IV. COMPARATIVE ANALYSIS

##### A. Dataset description

We used CBIS-DDSM Breast Cancer Image Dataset [24],

The dataset comprises 2,620 digitally scanned film mammography studies, among them 753 calcification cases. CBIS-DDSM encompasses verified pathology information across normal, benign, and malignant cases. The extensive size of the database, coupled with its validated ground truth, renders it a valuable asset for the advancement and evaluation of decision support systems. As IP-UNet and 3D-UNet are supposed to be trained using 3D volumes, we have converted the CT scans to NIFTI data format [25] using dicom2nifti python library <sup>1</sup>.

Figure 3 shows an example of a CT scan displayed in ITK-SNAP. The dataset statistics are shown in Table II.

<sup>1</sup>www.github.com/icometrix/dicom2nifti

##### B. Experiment settings

##### C. Result analysis

As mentioned earlier, we have compared IP-UNet with the conventional UNet, and a 3D-UNet. The architectures of the baselines have been set as follows: (1) UNet: Each DICOM slice is inputted into 2D UNet as defined in Table I. The segmentation output of all DICOM series is merged into a single 3D image and compared with the ground-truth annotation to compute the Dice score similarity. (2) 3D-UNet: Implemented 3D-UNet model that takes the NIFTI 3D as input (nii file), or an aggregated dicom series as input. The patch size is 512X512X128, and the initial learning rate was  $10^{-3}$ . IP-UNet and both baselines have been trained for 1000 epochs. All experiments were conducted with Alienware workstation with Intel(R) Core(TM) i7-8700K CPU @ 3.70GHz, equipped with 2 GPUs (GTX 1080 Ti).

##### D. Evaluation metrics

We used Precision, Recall and Dice Similarity Coefficient (DSC) as the evaluation metrics.

**Precision:** also known as sensitivity, and it refers to the proportion of positives that are correctly identified compared to the ground truth, and is computed as shown in (6), where  $TP$  is the number of true positives and  $FN$  is the number of false negatives.

$$Precision = \frac{TP}{TP + FN} \quad (6)$$

**Recall:** also known as specificity, and it measures the proportion of negatives that were correctly predicted, and is

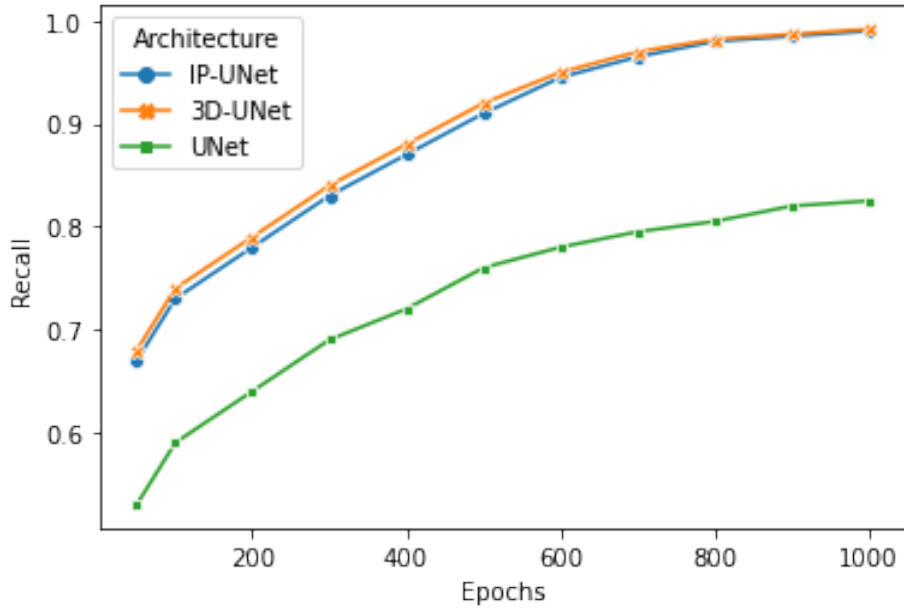


Fig. 4: Recall comparison results

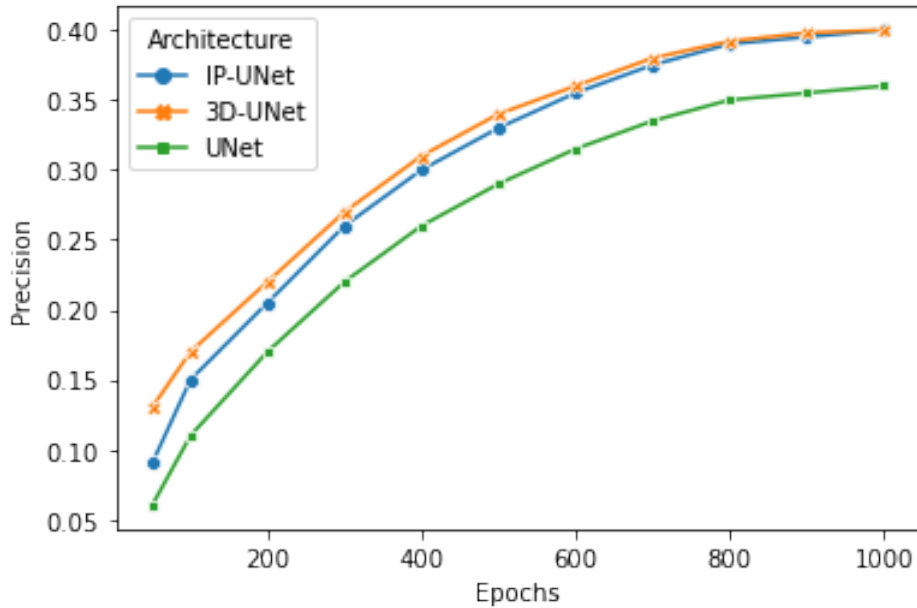


Fig. 5: Precision comparison results

computed as shown in (7), where  $TN$  is the number of true negatives and  $FP$  is the number of false positives.

$$recall = \frac{TN}{TN + FP} \tag{7}$$

**DSC:** is used to quantify the similarity between the predicted segmentation and the ground truth annotations, and is computed as shown in (8), where  $TP$  is the number of true positives,  $FN$  is the number of false negatives

$$DSC = \frac{2|P \cap P'|}{|P| + |P'|} = \frac{2TP}{2TP + FN + FP} \tag{8}$$

Figure 4, Figure 5 and Figure 6 compare IP-UNet to other baselines in terms of recall, precision and DSC respectively. In Figure 4, all architectures have relatively low recall when trained for less than 500 epochs. After that they significantly improve, to finally stabilize after 750 epochs. 3D-UNet and IP-UNet have much higher recall compared to the conventional 2D UNet. 3D-UNet and IP-UNet score recall of 99%, while 2D UNet scores as low as 82%. Such high recall achieved by 3D-UNet and IP-UNet is misleading, as precision does not take FN into account, and in our case, the proportion of calcified voxels among overall annotation voxels is very low, this results in a very high recall but low precision.

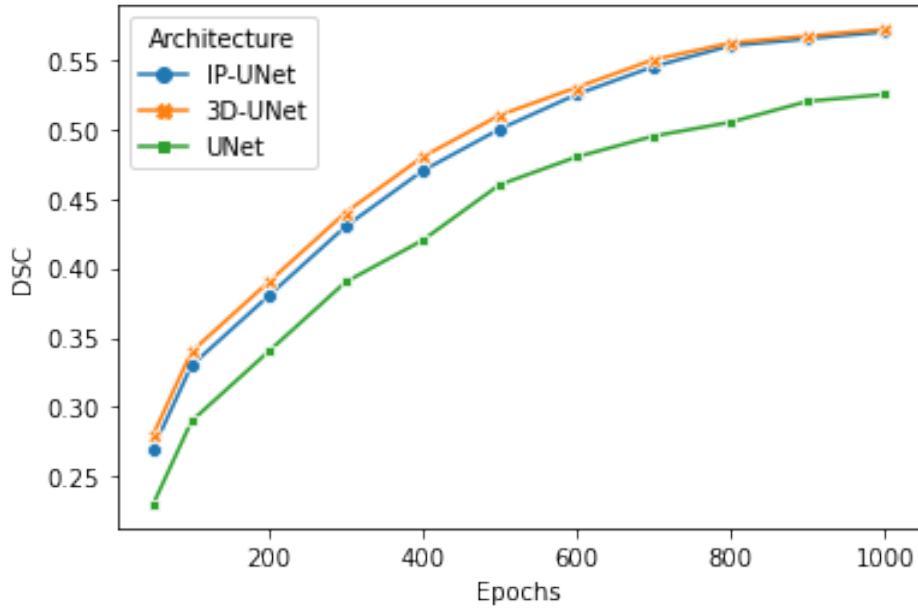


Fig. 6: DSC comparison results

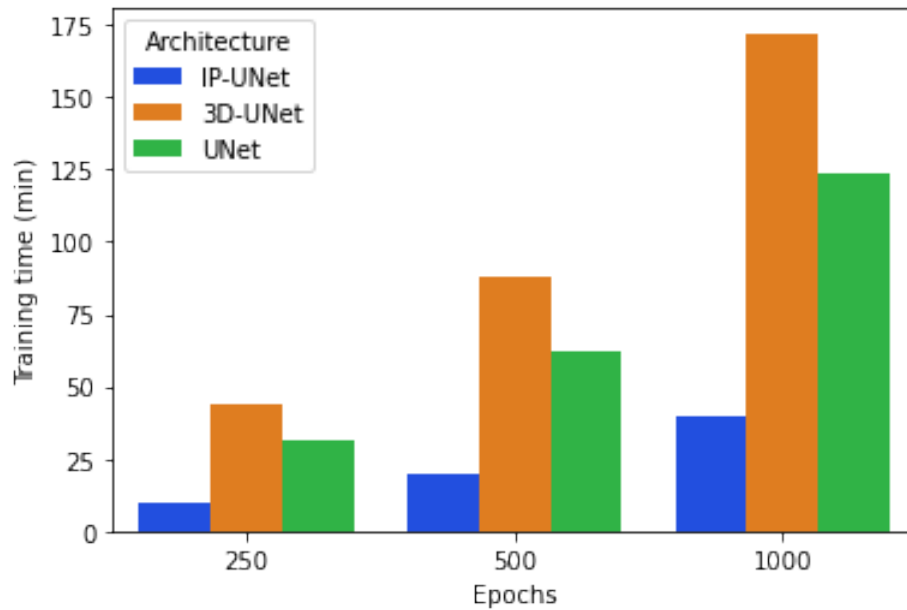


Fig. 7: Training time comparison

Figure 5 shows the precision of IP-UNet compared to the studied baselines. Again, 3D-UNet and IP-UNet have much higher precision compared to the conventional 2D UNet. But 3D-UNet and IP-UNet score just about 40% due to the high FN cases, especially for low calcification patients. Finally, Figure 6 shows the DSC for UNet, 3D-UNet and IP-UNet, the latter scores 57% when trained for more than 750 epochs. Table III shows the final recall, precision and DSC of the studied architecture when trained for 1000 epochs.

Although our proposed architecture IP-UNet has similar recall, precision and DSC with 3D-UNet, nonetheless, it is much more computationally efficient as it is trained with intensity

TABLE III: Sensitivity, specificity and Dice similarity coefficient

System	Recall	Precision	DSC
IP-UNet	0.99	0.4	0.525
UNet	0.825	0.36	0.525
3D-UNet	0.992	0.4	0.572

projections rather than the full 3D volumic data. Figure 7 shows the required training time for IP-UNet, 3D-UNet and 2D UNet respectively. IP-UNet maintains low training time, even when the model is trained with 1000 epochs. Unlike 3D-UNet and 2D UNet where the training time exponentially

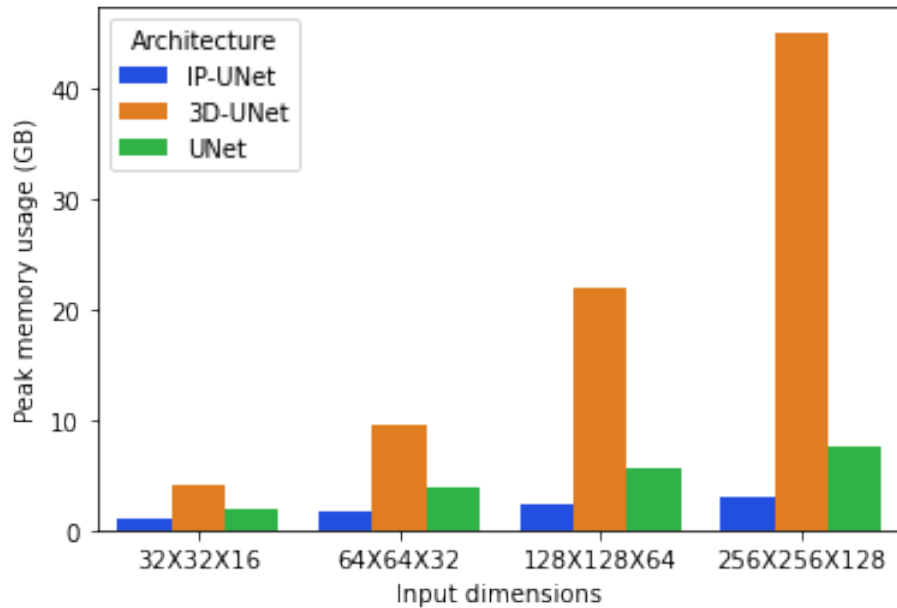


Fig. 8: Memory requirement comparison

increases in proportion to the increase of training epochs. Similarly, Figure 8 shows the average memory consumption of the studied models. Memory consumption was measured using tracemalloc Python package, and the values presented in Figure 8 are the average of 10 training cycles.

## V. CONCLUSION

In this paper, we have proposed IP-UNet, an end-to-end deep learning model that operates on intensity projections of 3D volumes instead of memory-consuming 3D volumetric data. IP-UNet can be trained with limited memory capability without loss of resolution of the original 3D images. We compared the performance of IP-UNet in terms of segmentation accuracy and computational cost with similar baselines, namely, UNet and 3D-UNet. In the experiment, we trained and evaluated IP-UNet on 500 3D volumetric images for automatic breast calcification detection. Results show that IP-UNet can achieve similar segmentation accuracy with 3D-UNet, and reduces the training time by 70%, and memory requirement by 92%.

## ACKNOWLEDGMENT

This work was supported by: The Insight Centre for Data Analytics funded by Science Foundation Ireland under Grant Number 12/RC/2289 P2.

## REFERENCES

- [1] N. Tajbakhsh, J. Y. Shin, S. R. Gurudu, R. T. Hurst, C. B. Kendall, M. B. Gotway, and J. Liang, "Convolutional neural networks for medical image analysis: Full training or fine tuning?" *IEEE transactions on medical imaging*, vol. 35, no. 5, pp. 1299–1312, 2016.
- [2] O. Ronneberger, P. Fischer, and T. Brox, "U-net: Convolutional networks for biomedical image segmentation," in *International Conference on Medical image computing and computer-assisted intervention*. Springer, 2015, pp. 234–241.
- [3] K. Kamnitsas, C. Ledig, V. F. Newcombe, J. P. Simpson, A. D. Kane, D. K. Menon, D. Rueckert, and B. Glocker, "Efficient multi-scale 3d cnn with fully connected crf for accurate brain lesion segmentation," *Medical image analysis*, vol. 36, pp. 61–78, 2017.
- [4] Ö. Çiçek, A. Abdulkadir, S. S. Lienkamp, T. Brox, and O. Ronneberger, "3d u-net: learning dense volumetric segmentation from sparse annotation," in *International conference on medical image computing and computer-assisted intervention*. Springer, 2016, pp. 424–432.
- [5] D. Ojika, B. Patel, G. A. Reina, T. Boyer, C. Martin, and P. Shah, "Addressing the memory bottleneck in AI model training," *arXiv preprint*, vol. abs/2003.08732, 2020. [Online]. Available: <https://arxiv.org/abs/2003.08732>
- [6] S. Zheng, J. Guo, X. Cui, R. N. Veldhuis, M. Oudkerk, and P. M. Van Ooijen, "Automatic pulmonary nodule detection in ct scans using convolutional neural networks based on maximum intensity projection," *IEEE transactions on medical imaging*, vol. 39, no. 3, pp. 797–805, 2019.
- [7] T. Fujioka, Y. Yashima, J. Oyama, M. Mori, K. Kubota, L. Katsuta, K. Kimura, E. Yamaga, G. Oda, T. Nakagawa *et al.*, "Deep-learning approach with convolutional neural network for classification of maximum intensity projections of dynamic contrast-enhanced breast magnetic resonance imaging," *Magnetic Resonance Imaging*, vol. 75, pp. 1–8, 2021.
- [8] T. Akai, D. Taniguchi, R. Oda, M. Asada, S. Toyama, D. Tokunaga, T. Seno, Y. Kawahito, Y. Fujii, H. Ito *et al.*, "Prediction of radiographic progression in synovitis-positive joints on maximum intensity projection of magnetic resonance imaging in rheumatoid arthritis," *Clinical rheumatology*, vol. 35, no. 4, pp. 873–878, 2016.
- [9] H. Zhang, E. S. Ingham, M. K. J. Gagnon, L. M. Mahakian, J. Liu, J. L. Foiret, J. K. Willmann, and K. W. Ferrara, "In vitro characterization and in vivo ultrasound molecular imaging of nucleolin-targeted microbubbles," *Biomaterials*, vol. 118, pp. 63–73, 2017.
- [10] C. Booz, T. J. Vogl, U. J. Schoepf, D. Caruso, M. C. Inserra, I. Yel, S. S. Martin, A. M. Bucher, L. Lenga, D. Caudo *et al.*, "Value of minimum intensity projections for chest ct in covid-19 patients," *European Journal of Radiology*, vol. 135, p. 109478, 2021.
- [11] M. Kozinski, A. Mosinska, M. Salzmann, and P. Fua, "Tracing in 2D to reduce the annotation effort for 3D deep delineation of linear structures," *Medical Image Analysis*, vol. 60, p. 101590, feb 2020.
- [12] —, "Learning to segment 3D linear structures using only 2D annotations," *Lecture Notes in Computer Science*, vol. 11071 LNCS, pp. 283–291, 2018.
- [13] C. Wang, T. MacGillivray, G. Macnaught, G. Yang, and D. Newby, "A two-stage 3D Unet framework for multi-class segmentation on full resolution image," apr 2018. [Online]. Available: <https://arxiv.org/abs/1804.04341v1>

- [14] S. Zheng, X. Cui, M. Vonder, R. N. Veldhuis, Z. Ye, R. Vliegthart, M. Oudkerk, and P. M. van Ooijen, "Deep learning-based pulmonary nodule detection: Effect of slab thickness in maximum intensity projections at the nodule candidate detection stage," *Computer methods and programs in biomedicine*, vol. 196, p. 105620, 2020.
- [15] S. Zheng, J. Guo, X. Cui, R. N. Veldhuis, M. Oudkerk, and P. M. Van Ooijen, "Automatic pulmonary nodule detection in ct scans using convolutional neural networks based on maximum intensity projection," *IEEE transactions on medical imaging*, vol. 39, no. 3, pp. 797–805, 2019.
- [16] T. Fujioka, Y. Yashima, J. Oyama, M. Mori, K. Kubota, L. Katsuta, K. Kimura, E. Yamaga, G. Oda, T. Nakagawa *et al.*, "Deep-learning approach with convolutional neural network for classification of maximum intensity projections of dynamic contrast-enhanced breast magnetic resonance imaging," *Magnetic Resonance Imaging*, vol. 75, pp. 1–8, 2021.
- [17] K. Takahashi, T. Fujioka, J. Oyama, M. Mori, E. Yamaga, Y. Yashima, T. Imokawa, A. Hayashi, Y. Kujiraoka, J. Tsuchiya *et al.*, "Deep learning using multiple degrees of maximum-intensity projection for pet/ct image classification in breast cancer," *Tomography*, vol. 8, no. 1, pp. 131–141, 2022.
- [18] L. Wang, L. Chang, R. Luo, X. Cui, H. Liu, H. Wu, Y. Chen, Y. Zhang, C. Wu, F. Li *et al.*, "An artificial intelligence system using maximum intensity projection mr images facilitates classification of non-mass enhancement breast lesions," *European Radiology*, pp. 1–11, 2022.
- [19] A. Song, L. Xu, L. Wang, B. Wang, X. Yang, B. Xu, B. Yang, and S. E. Greenwald, "Automatic coronary artery segmentation of ccta images with an efficient feature-fusion-and-rectification 3d-unet," *IEEE Journal of Biomedical and Health Informatics*, vol. 26, no. 8, pp. 4044–4055, 2022.
- [20] Y. Lei, B. Guo, Y. Fu, T. Wang, T. Liu, W. Curran, L. Zhang, and X. Yang, "Automated coronary artery segmentation in coronary computed tomography angiography (ccta) using deep learning neural networks," in *Medical Imaging 2020: Imaging Informatics for Healthcare, Research, and Applications*, vol. 11318. SPIE, 2020, pp. 279–284.
- [21] A. K. Dubey and V. Jain, "Comparative study of convolution neural network's relu and leaky-relu activation functions," in *Applications of Computing, Automation and Wireless Systems in Electrical Engineering: Proceedings of MARC 2018*. Springer, 2019, pp. 873–880.
- [22] W. Zhang, Y. Wu, B. Yang, S. Hu, L. Wu, and S. Dhelim, "Overview of multi-modal brain tumor mr image segmentation," MDPI, p. 1051, 2021.
- [23] U. Kamal, T. I. Tonmoy, S. Das, and M. K. Hasan, "Automatic traffic sign detection and recognition using segunet and a modified tversky loss function with 11-constraint," *IEEE Transactions on Intelligent Transportation Systems*, vol. 21, no. 4, pp. 1467–1479, 2019.
- [24] R. S. Lee, F. Gimenez, A. Hoogi, K. K. Miyake, M. Gorovoy, and D. L. Rubin, "A curated mammography data set for use in computer-aided detection and diagnosis research," *Scientific data*, vol. 4, no. 1, pp. 1–9, 2017.
- [25] X. Li, P. S. Morgan, J. Ashburner, J. Smith, and C. Rorden, "The first step for neuroimaging data analysis: Dicom to nifti conversion," *Journal of neuroscience methods*, vol. 264, pp. 47–56, 2016.



Computer Systems.

**Mohand Tahar Kechadi** is a full professor in school of computer science, University College Dublin, Ireland. He received master's and Ph.D. degrees in computer science from the University of Lille 1, France. His research interests include data mining, distributed data mining heterogeneous distributed systems, grid and cloud computing, and digital forensics and cyber-crime investigations. He is a member of the Communications of the ACM journal and IEEE Computer Society. He is an Editorial Board Member of journal of Future Generation



**Liming Chen** is a professor in the School of Computer Science and Informatics at University of Ulster, Newtownabbey, United Kingdom. He received his B.Eng and M.Eng from Beijing Institute of Technology (BIT), Beijing, China, and his Ph.D in Artificial Intelligence from De Montfort University, UK. His research interests include data analysis, ubiquitous computing, and human-computer interaction. Liming is a Fellow of IET, a Senior Member of IEEE, a Member of the IEEE Computational Intelligence Society (IEEE CIS), a Member of the IEEE CIS Smart World Technical Committee (SWTC), and the Founding Chair of the IEEE CIS SWTC Task Force on User-centred Smart Systems (TF-UCSS). He has served as an expert assessor, panel member and evaluator for UK EPSRC (Engineering and Physical Sciences Research Council, member of the Peer Review College), ESRC (Economic and Social Science Research Council), European Commission Horizon 2020 Research Program, Danish Agency for Science and Higher Education, Denmark, Canada Foundation for Innovation (CFI), Canada, Chilean National Science and Technology Commission (CONICYT), Chile, and NWO (The Netherlands Organisation for Scientific Research), Netherlands.



**Sahraoui Dhelim** is a senior postdoctoral researcher at University College Dublin, Ireland. He was a visiting researcher at Ulster University, UK (2020–2021). He obtained his PhD degree in Computer Science and Technology from the University of Science and Technology Beijing, China, in 2020. And a Master's degree in Networking and Distributed Systems from the University of Laghouat, Algeria, in 2014. And Bs degree in computer science from the University of Djelfa, in 2012. He is a guest editor in several reputable journals, including Electronics Journal and Applied Sciences Journal. His research interests include Social Computing, Smart Agriculture, Deep-learning, Recommendation Systems and Intelligent Transportation Systems.



Transportation Systems.

**Nyothiri Aung** is a postdoctoral researcher at University College Dublin, Ireland. She received her PhD in Computer Science and Technology from University of Science and Technology Beijing, China, 2020. And a Master's of Information Technology from Mandalay Technological University, Myanmar, 2012. She worked as a demonstrator at the Department of Information Technology in Technological University of Meiktila, Myanmar (2008–2010). Her research interests include Social Computing, Medical image analysis, and Intelligent